Journal of Physics B: Atomic,
Molecular and Optical Physics

PAPER

Dissipative phase transition in an open Tavis–Cummings model with a two-photon drive

To cite this article: Kingshuk Adhikary *et al* 2023 *J. Phys. B: At. Mol. Opt. Phys.* **56** 135401

View the article online for updates and enhancements.

You may also like

- Effect of an external radiation field on the properties of the atoms and cavity field in the two-atom Tavis–Cummings model
Wang Zhong-Chun, Wang Qi, Zhang Yong-Sheng et al.
- Entanglement in Three-Atom Tavis–Cummings Model Induced by a Thermal Field
Cai Jin-Fang and Liu Hui-Ping
- Time evolution of the atomic inversion for the generalized Tavis–Cummings model—QIM approach
N M Bogoliubov, I Ermakov and A Rybin



This content was downloaded from IP address 88.255.99.30 on 12/02/2024 at 16:58

IOP Publishing Journal of Physics B: Atomic, Molecular and Optical Physics
J. Phys. B: At. Mol. Opt. Phys. **56** (2023) 135401 (10pp) https://doi.org/10.1088/1361-6455/acdc6e

Dissipative phase transition in an open Tavis–Cummings model with a two-photon drive

Kingshuk Adhikary[1], **Özgür E Müstecaplıoğlu**[2,3] **and Bimalendu Deb**[1,*]

[1] School of Physical Sciences, Indian Association for the Cultivation of Science, Jadavpur, Kolkata 700032, India
[2] Department of Physics, Koç University, Sariyer, Istanbul 34450, Türkiye
[3] TÜBİTAK Research Institute for Fundamental Sciences, Gebze 41470, Türkiye

E-mail: msbd@iacs.res.in

Received 22 March 2023, revised 19 May 2023
Accepted for publication 7 June 2023
Published 30 June 2023

Abstract

We investigate the steady-state quantum phases and associated collective phenomena of an open Tavis–Cummings (TC) model driven by a two-photon source. The standard (non-dissipative) TC model describes the quantum phases of an ensemble of N_q two-level quantum emitters interacting with a single-mode electromagnetic field. The interplay among coherent driving, dissipation, and dipole interactions of the open TC model results in emergent collective phenomena, leading to a dissipative or non-equilibrium phase transition from the normal to the superradiant phase. We solve the Liouvillian equation analytically using the semi-classical mean-field approximation. We carry out stability analysis of the steady-state phases and determine the phase boundary. The use of Holstein–Primakoff transformation in the thermodynamic limit $N_q \to \infty$ reduces the system to an effective coupled-oscillator model, the solution of which yields collective modes.

Keywords: Dicke model, Tavis–Cummings model, dissipative phase transition, two-photon drive, quantum phase transition, Z_2 symmetry

(Some figures may appear in colour only in the online journal)

1. Introduction

Superradiant phase transition (SPT) [1–4] is a collective phenomenon in an ensemble of identical two-level emitters or atoms interacting with a single-mode light field described by the well-known Dicke model (DM) [5–7]. This model provides a useful platform for studying quantum phase transition (QPT) [8–13] in a variety of physical systems. The DM is reduced to the Tavis–Cummings (TC) model [14, 15] under the rotating wave approximation [16]. The DM has $\mathbb{Z}_2$ symmetry, while the TC model follows $U(1)$ symmetry. Both models are capable of exhibiting QPTs, but the DM has critical coupling that is twice that of the TC model [14, 15].

Over the years, controllable light-matter interacting systems [17–19] have become a key resource in the study of SPT [1–4, 7, 20–22]. The normal–SPT occurs not only in the TC model, but also in the Rabi [2, 23, 24] and the Jaynes–Cummings models [25]. Recently, a new class of SPTs has been found in a 'quantum Rabi triangle' with broken $\mathbb{Z}_2$ and chiral symmetry [26, 27]. The TC model exhibits a wide variety of interesting phenomena apart from SPT, such as spin squeezing [28, 29] and multi-photon transitions [30], many-body phenomena [9, 18, 31, 32], quantum discord [33, 34], quantum fluctuations [35, 36], and entanglement [37–41]. Although extensive theoretical studies on SPT in Dicke and

* Author to whom any correspondence should be addressed.

 © 2023 IOP Publishing Ltd

TC models have been carried out over the years, the experimental realization of SPT in a prototype or standard DM remains quite challenging, because achieving a super-strong critical coupling strength required for SPT is extremely difficult. However, the achievement of ultra- or super-strong coupling in the microwave frequency regime using superconducting circuit quantum electrodynamics (QED) seems to be possible. Recently, it has been theoretically shown that a complex quantum network can lead to super-strong atom–field interaction and high-temperature SPT [42, 43]. The quantum critical behaviour of a driven TC model using superconducting circuit QED [32] has been experimentally demonstrated. Dicke SPT has been experimentally observed in a superfluid Bose–Einstein condensate in a cavity, where two momentum states of the condensate form a two-level system [13].

Here, we study QPT and collective phenomena in a dissipative TC model consisting of N two-level emitters inside a single-mode cavity driven by a two-photon drive. We analyze the system from two distinct perspectives: (i) ground-state analysis of the driven system in the absence of dissipation; and (ii) the steady-state properties of the driven dissipative system. We consider a parametric two-photon drive, $G(\hat{a}^{\dagger 2}+\hat{a}^2)$, as used in a recent study [36], to show the effect of the spontaneous breaking of $U(1)$ symmetry on the system. The advantage of the two-photon drive is that it enables SPT even without ultrastrong coupling. This nonlinear drive can be realized by pumping an intracavity crystal with second-order nonlinearity with an external laser with a frequency that is equal to twice the cavity frequency [36]. This leads to an optical parametric amplification process and squeezing, whereby a single laser photon generates two cavity photons, thereby breaking the U(1) symmetry of the system. Similar parametric nonlinear pumping is also considered to study QPT in an extended DM [44]. We first obtain the ground-state energy spectrum of the model at zero temperature, revealing the phase transition with the critical coupling $\lambda_c=\sqrt{\Delta_q\Delta_r}$ [7, 31, 45], where $\Delta_{r(q)}$ is the cavity (atom) detuning from the drive frequency. We then introduce into the driven system both atomic and cavity dissipation, which make the system essentially non-equilibrium. The inclusion of atomic decay breaks the spin conservation of the ensemble of the emitters, unlike that in [36]. Based on a semi-classical analysis under the mean-field approximation, a rich phase diagram of non-equilibrium phases and phase boundaries is obtained. By performing stability analysis, we characterize the nature of the normal and superradiant phases. Our results show how the atomic decay affects both the critical coupling strength and the boundary conditions.

Next, by employing the bosonization method in the thermodynamic limit $N_q\to\infty$ under the Holstein–Primakoff (HP) transformation [46, 47], we replace the collective spin operator of the atoms with a single bosonic operator. As a result, the system effectively reduces to the model of a pair of coupled harmonic oscillators [48, 49] that also shows the SPT. The Green's function formalism is used to determine the critical strength of this reduced model. To the best of our knowledge, the driven dissipative TC model under consideration and the model of a pair of coupled harmonic oscillators have never been connected, particularly within the context of open quantum systems [50–52].

The layout of this paper is as follows. Our driven dissipative TC model is described in section 2. In section 3, we describe the dissipative normal–SPT of the system. Finally, in section 4, we conclude and give an outlook on our study.

2. The model

An ensemble of non-interacting two-level atoms that are collectively coupled to a common cavity resonator constitutes a typical TC model, see figure 1 for an example. Since we are only interested in the weak coupling regime, the counter-rotating terms are not considered. In the presence of a two-photon (parametric) source that drives off the resonator, the Hamiltonian is $\hat{H}(t)=\hat{H}_{\rm TC}+\hat{H}_{\rm drive}(t)$ where we set $\hbar=1$ thereafter

$$\hat{H}_{\rm TC}=\omega_r\hat{a}^\dagger\hat{a}+\omega_q\sum_{i=1}^{N_q}\frac{\hat{\sigma}_{z,i}}{2}+\frac{\lambda}{\sqrt{N_q}}\sum_{i=1}^{N_q}(\hat{a}^\dagger\hat{\sigma}_{-,i}+\hat{a}\hat{\sigma}_{+,i}) \quad (1)$$

$$\hat{H}_{\rm drive}(t)=\frac{G}{2}\left(\hat{a}^{\dagger 2}e^{-i2\omega_p t}+\hat{a}^2e^{i2\omega_p t}\right) \quad (2)$$

where G and ω_p are the pump amplitude and frequency, respectively. Here, $\hat{a}(\hat{a}^\dagger)$ is the annihilation(creation) operator of a photon in the cavity mode, $\hat{\sigma}_{a,i}(a=x,y,z,+,-)$ are the usual Pauli's spin matrices in the Hilbert space of the i-th qubit, ω_r is the frequency of the field, ω_q is the energy level splitting of each atom, and $\lambda>0$ is the atom-field coupling strength. The factor $1/\sqrt{N_q}$, which normalizes the interaction, is necessary to go for a well defined thermodynamic limit $N_q\to\infty$ [7].

One can replace atomic degrees-of-freedom with the total spin angular momentum (collective) operators, given by

$$\hat{J}_\alpha=\sum_{\alpha=x,y,z;i=1}^{N_q}\frac{\hat{\sigma}_{\alpha,i}}{2};\qquad \hat{J}_\pm=\sum_{i=1}^{N_q}\hat{\sigma}_{\pm,i}. \quad (3)$$

They obey the commutation algebra $[\hat{J}_\alpha,\hat{J}_\beta]=i\epsilon_{\alpha\beta\gamma}\hat{J}_\gamma, [\hat{J}_z,\hat{J}_\pm]=\pm\hat{J}_\pm, [\hat{J}_+,\hat{J}_-]=2\hat{J}_z$.

The Hamiltonian, equation (1), then takes the form

$$\hat{H}_{\rm TC}=\omega_r\hat{a}^\dagger\hat{a}+\omega_q\hat{J}_z+\frac{\lambda}{\sqrt{N_q}}\left(\hat{a}\hat{J}_++\hat{a}^\dagger\hat{J}_-\right) \quad (4)$$

which satisfies $[\hat{H}_{\rm TC},\hat{J}^2]=0$, where $\hat{J}=\sqrt{\hat{J}_x^2+\hat{J}_y^2+\hat{J}_z^2}$ is the total spin angular momentum operator.

To eliminate the explicit time dependence of the Hamiltonian $\hat{H}_{\rm drive}(t)$, we may write it in a reference frame rotating at the pump frequency ω_p and performing the unitary transformation $\hat{U}(t)=e^{-i(\omega_p\hat{a}^\dagger\hat{a}+\omega_p\hat{J}_z)t}$; the effective

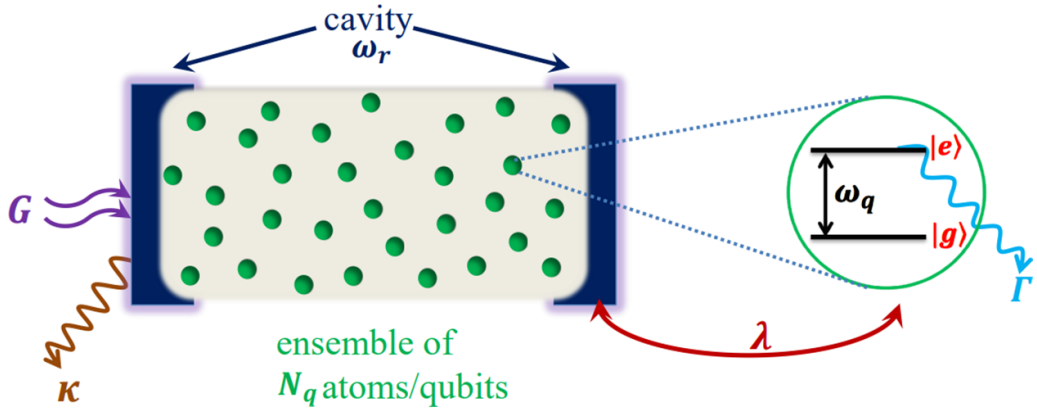


Figure 1. A schematic diagram of an open DM consisting of an ensemble of N_q identical qubits inside a single-mode cavity. The strength of the cavity–qubit coupling is λ, and the cavity is pumped by a two-photon parametric drive with strength G. The frequencies of the cavity and the atomic transition are denoted by ω_r and ω_q, respectively. Here, κ and Γ are the decay rates of cavity photons and atoms, respectively.

Hamiltonian of the system in the interaction picture takes the form

$$\hat{H}_{\rm eff} = \Delta_r \hat{a}^\dagger \hat{a} + \Delta_q \hat{J}_z + \frac{\lambda}{\sqrt{N_q}}\left(\hat{a}\hat{J}_+ + \hat{a}^\dagger \hat{J}_-\right) + \frac{G}{2}\left(\hat{a}^{\dagger 2} + \hat{a}^2\right), \tag{5}$$

where $\Delta_q = \omega_q - \omega_p$ ($\Delta_r = \omega_r - \omega_p$) is the detuning of a qubit (resonator) resonance from the drive frequency.

In the absence of the drive ($G = 0$), the Hamiltonian, equation (5), possesses a continuous $U(1)$ symmetry for the transformation $(\hat{a}, \hat{J}_+) \to (\hat{a}e^{i\phi}, \hat{J}_+ e^{-i\phi})$. However, in the presence of coherent pumping ($G \neq 0$), the $U(1)$ symmetry is lifted.

We include the effects of the coupling of the qubits and the resonator to the environment under the Born–Markov approximation, resulting in the loss of cavity photons with rate κ and the relaxation of the qubits with rate Γ. The time evolution of the system is described by the standard quantum master equation

$$\frac{{\rm d}\hat{\rho}}{{\rm d}t} = -i\left[\hat{H}_{\rm eff}, \hat{\rho}\right] + \frac{\kappa}{2}\mathcal{D}[\hat{a}]\hat{\rho} + \frac{\Gamma}{2}\mathcal{D}[\hat{J}_-]\hat{\rho}, \tag{6}$$

for the density operator $\hat{\rho}$ of the system. Here, the commutator describes the coherent evolution of our system, and the Lindblad dissipator for an arbitrary operator $\hat{\mathcal{O}}$ is given by $\mathcal{D}[\hat{\mathcal{O}}]\hat{\rho} = (2\hat{\mathcal{O}}\hat{\rho}\hat{\mathcal{O}}^\dagger - \hat{\mathcal{O}}^\dagger\hat{\mathcal{O}}\hat{\rho} - \hat{\rho}\hat{\mathcal{O}}^\dagger\hat{\mathcal{O}})$ that describes various loss processes. To describe the dissipative processes of the resonator, we use the usual Lindblad terms

$$\begin{aligned}\mathcal{D}[\hat{a}]\hat{\rho} = (N_{\rm th}+1)\left(2\hat{a}\hat{\rho}\hat{a}^\dagger - \left\{\hat{a}^\dagger\hat{a}, \hat{\rho}\right\}\right) \\ + N_{\rm th}\left(2\hat{a}^\dagger\hat{\rho}\hat{a} - \left\{\hat{a}\hat{a}^\dagger, \hat{\rho}\right\}\right),\end{aligned} \tag{7}$$

where $N_{\rm th} = \left(\exp\left(\frac{\omega_c}{k_B T}\right) - 1\right)^{-1}$ is the thermal number of photons in the resonator. More precisely, the first term describes the emission of photons to the environment, while the second term accounts for the absorption of thermal photons by the resonator.

Similarly, for the qubit, the decay of atoms from the excited state to the ground state is described as follows

$$\mathcal{D}[\hat{J}_-]\hat{\rho} = \left(2\hat{J}_-\hat{\rho}\hat{J}_+ - \left\{\hat{J}_+\hat{J}_-, \hat{\rho}\right\}\right). \tag{8}$$

3. Results and discussion

We first analyze the ground-state characteristics of the driven TC model without any dissipation. We then discuss the results for the driven dissipative TC model.

3.1. Ground-state properties

The ground state has versatile physical characteristics, unlike the higher eigenstates of the Hamiltonian, equation (5). We solve the eigenvalue equation

$$\hat{H}_{\rm eff}|\Psi\rangle = E|\Psi\rangle, \tag{9}$$

with the eigenvalue E for the entire Hilbert space: $|\Psi\rangle \equiv \{|j,m\rangle \otimes |N_p\rangle\}$, where $|j,m\rangle$ is a Dicke state or collective spin state and $|N_p\rangle$ is a conventional Fock basis state of bosons (photons) satisfying $\hat{a}^\dagger\hat{a}|N_p\rangle = N_p|N_p\rangle$ with $N_p \in \{0,1,2,\ldots\}$. The Dicke states explicitly satisfy,

$$\hat{J}^2|j,m\rangle = j(j+1)|j,m\rangle, \tag{10}$$

$$\hat{J}_z|j,m\rangle = m|j,m\rangle, \tag{11}$$

$$\hat{J}_\pm|j,m\rangle = \sqrt{(j\mp m)(j\pm m+1)}|j,m\pm 1\rangle, \tag{12}$$

with $j = \{N_q/2, N_q/2-1, \ldots, -N_q/2+1, -N_q/2\}$, and $m = \{j, j-1, \ldots, -j+1, -j\}$. Here, we define $j = |N_q/2|$ as the length of the pseudospin for an ensemble of N_q-qubits with the dimension being equal to (N_q+1). Here, N_q may be even or odd. We also truncate the size of the Fock basis to a finite value, e.g. N_p^{max}. Thus, the dimension of the Hilbert space

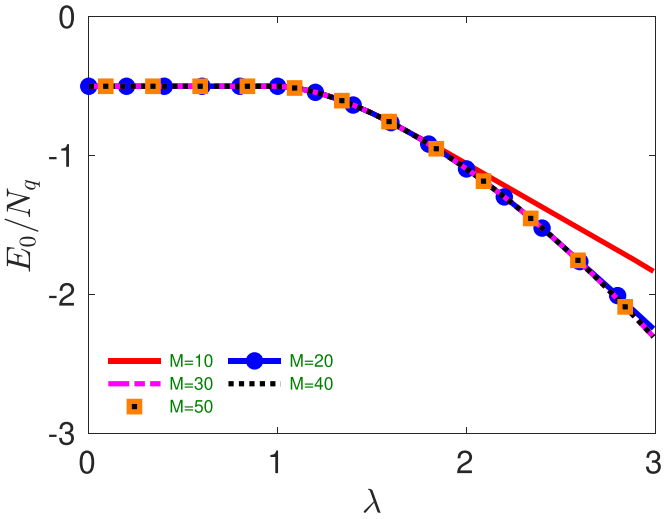


Figure 2. The ground-state energy eigenvalue of the isolated driven TC model is plotted as a function of λ for several dimensions M of the Hilbert space of the cavity photons. All the coupling constants are scaled by $\Delta_q = \Delta_r = \Delta$.

is $(N_q+1)(N_p^{\max}+1)$. We have chosen the dimension (values of N_q and N_p) of the Hilbert space judicially, such that $|E(N_p+10)-E(N_p)|/N_q \simeq 0$ becomes negligible. We examine the convergence of energy eigenvalues against the variation of $M = N_p^{max}$ in figure 2. In figure 2, we show the expectation value (normalized by N_q) of the ground-state energy $E_0 = \langle \hat{H}_{\rm eff}\rangle$, evaluated numerically using equation (5). The ground-state energy is found to converge as we increase the size of the cavity Fock basis M beyond a certain value. At the critical strength $\lambda = \lambda_c$, we notice a phase transition as E_0/N_q remains constant up to $\lambda \leqslant \lambda_c$, and beyond λ_c it changes. It is to be pointed out that the higher eigenvalues have similar characteristics. For our numerical analysis, we fix $N_q = 10$ and $N_p^{max} = 30$ to ensure the convergence of our results. We set the detuning $(\Delta_q = \Delta_r)$ as the unit of energy. We diagonalize the Hamiltonian, equation (5), numerically using the Qutip code [53].

We demonstrate, in figure 3, the average value of the cavity photon number and the atomic inversion for the ground state. When $G = 0$, the characteristics of the atomic inversion $\langle \hat{J}_z\rangle/N_q$ and cavity photon number $\langle \hat{a}^\dagger \hat{a}\rangle/N_q$ change at $\lambda_c = 1$. Therefore, this feature implies a QPT of the system without drive. For an intermediate drive $(G = 0.5)$, the driven system exhibits phase transition at a lower value of $\lambda(<1)$. In the presence of the larger drive $G = 1$, the system always exhibits the QPT without any threshold. The average value of $\langle \hat{J}_z\rangle/N_q \neq -0.5 < 0$ corresponds to a post-phase-transition situation. We compare the normal–SPT with the QPT.

3.2. *The effects of dissipation: semi-classical steady-states*

We define an analogue of the thermodynamic limit by $N_q \to \infty$. The scaled mean values of the operators $\hat{\mathcal{O}} \in (\hat{a}, \hat{J}_x, \hat{J}_y, \hat{J}_z)$ are defined by

$$\psi = \frac{\langle \hat{a}\rangle}{\sqrt{N_q}}, X = \frac{\langle \hat{J}_x\rangle}{N_q}, Y = \frac{\langle \hat{J}_y\rangle}{N_q}, Z = \frac{\langle \hat{J}_z\rangle}{N_q}. \tag{13}$$

For mathematical simplicity, one can define the quadrature variables of the cavity field $Q = (\psi + \psi^*)/\sqrt{2}$ and $P = (\psi - \psi^*)/i\sqrt{2}$ to ensure that all the variables are real quantities, i.e. $\langle \hat{\mathcal{O}}\rangle \in \mathbb{R}$. Under the mean-field approximation [54], we may write $\hat{\mathcal{O}} \simeq \langle \hat{\mathcal{O}}\rangle$, with fluctuation $\delta\hat{\mathcal{O}} = 0$. We use equations (5) and (6) to derive the Heisenberg equations of motion

$$\begin{cases} \partial_t Q = (\Delta_r - G)P - \frac{\kappa}{2}Q - \sqrt{2}\lambda Y, \\ \partial_t P = -(\Delta_r + G)Q - \frac{\kappa}{2}P - \sqrt{2}\lambda X, \\ \partial_t X = -\delta_q Y - \sqrt{2}\lambda ZP - \frac{\Gamma}{2}X, \\ \partial_t Y = \delta_q X - \sqrt{2}\lambda ZQ - \frac{\Gamma}{2}Y, \\ \partial_t Z = \sqrt{2}\lambda(PX + QY) - \frac{\Gamma}{2}(1+2Z). \end{cases} \tag{14}$$

These five-dimensional semi-classical (mean-field) equations completely determine the evolution dynamics of the driven TC model. Under the steady-state approximation, $\partial_t\langle O\rangle = 0$.

One steady-state solution of equation (14) is characterized by

$$Q_{NP} = 0, P_{NP} = 0, X_{NP} = 0, Y_{NP} = 0, Z_{NP} = -\frac{1}{2}. \tag{15}$$

Here, the subscript '*NP*' stands for the normal phase of the system. These normal phase solutions imply no excitation in the cavity mode, and all the atomic spins are in the spin-down state.

However, another solution to equation (14) is

$$\begin{cases} Z_{SP,\pm} = \left[\frac{\kappa\Gamma}{4} - \Delta_q(\Delta_r - G)\right] + \frac{1}{4\lambda^2 r_\pm}\left[\Delta_q\kappa + \Gamma(\Delta_r + G)\right], \\ Q_{SP,\pm} = \pm\sqrt{\frac{-\Gamma(1+2Z_{SP,\pm})}{4Gr_\pm + \kappa(1+r_\pm^2)}}, \\ P_{SP,\pm} = Q_{SP,\pm}r_\pm, \\ X_{SP,\pm} = -\frac{Q_{SP,\pm}}{2\sqrt{2}\lambda}\left[2(\Delta_r + G) + \kappa r_\pm\right], \\ Y_{SP,\pm} = \frac{Q_{SP,\pm}}{2\sqrt{2}\lambda}\left[2(\Delta_r - G)r_\pm - \kappa\right], \end{cases} \tag{16}$$

where we introduce

$$r_\pm = \frac{-2G\Delta_q \pm \sqrt{\Delta_q^2(4G^2 - \kappa^2) + \Gamma^2(G^2 - \Delta_r^2) - 2\kappa\Gamma\Delta_q\Delta_r}}{\kappa\Delta_q + \Gamma(\Delta_r - G)} \tag{17}$$

and the subscript '*SP*' stands for the superradiant phase of the system. Indeed, the non-zero value of $(Z+1/2)$ indicates the normal–superradiant transition at the steady state, while $Z = -1/2$ implies that all the atoms are in the ground state: that is, the system is in the normal state. Specifically, the boundary of this phase transition is determined by the solution $Z = -\lambda_c^2/2\lambda^2$ with the critical coupling strength

$$\lambda_{c,\pm} = \pm\sqrt{\left(-\frac{\kappa\Gamma}{4} + \Delta_q(\Delta_r - G)\right) - \frac{1}{2r_\pm}\left(\Delta_q\kappa + \Gamma(\Delta_r + G)\right)}. \tag{18}$$

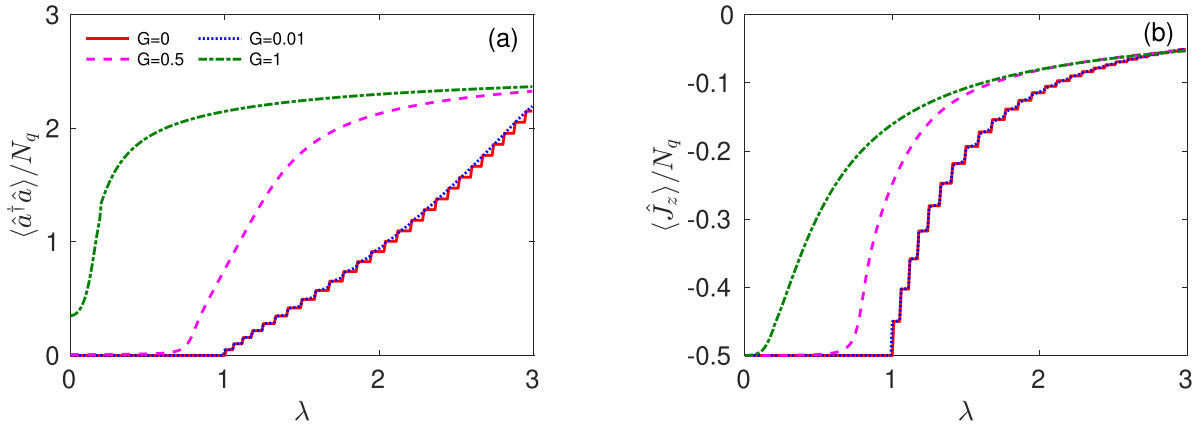


Figure 3. The normalized mean of (a) the cavity photon, and (b) atomic inversion as a function of λ for different values of drive G, as shown in the top left of plot (a).

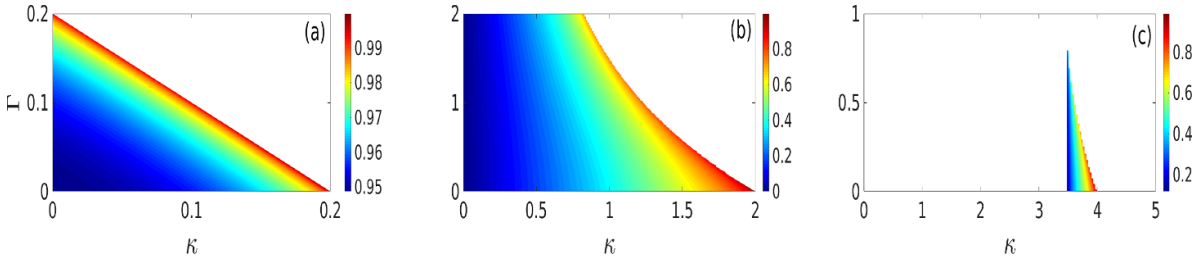


Figure 4. The critical coupling strength $\lambda_{c,-}$ is plotted in the dissipative plane (κ, Γ) with (a) $G = 0.1$, (b) $G = 1$, and (c) $G = 2$. The white part depicts the nonphysical nature of $\lambda_{c,-}$.

The appearance of $\pm$ in equation (18) is due to $r_\pm$. However, later we numerically work out the standard stability analysis thoroughly to ascertain stable physical solutions for the superradiant phase. From this stability point of view, only $\lambda_{c,-}$ is acceptable, and hence we discard the solution associated with $Z_{SP,+}$.

In figure 4, we show the characteristics of the critical value $\lambda_{c,-}$. This plot can very effectively explain the effects of decay rates on the normal–superradiant transition. For clarity, we show the validity regime of $\lambda_{c,-}$ for three different drive strengths G to illustrate the normal–superradiant phase transition (PT) and identify the corresponding phase boundary:

(i) For the small $G = 0.1$, we notice that the variation of $\lambda_{c,-}$ is negligible and remains constant: nearly $\lambda_{c,-} \simeq 1$. The decay rates should be varied to obtain the phase transition.
(ii) The variation of $\lambda_{c,-}$ for $G = 1$ is shown in figure 4(b). Here, $\lambda_{c,-}$ has a wide range of variation from 0 to 1 in the dissipative plane. In fact, this will offer an advantage to experimentally demonstrate the normal–superradiant transition.
(iii) In the presence of a stronger drive ($G = 2$), the system exhibits phase transition only for large values of κ. Experimental realization of the dissipative phase transition in this situation will be challenging because the system moves towards highly non-equilibrium states.

Figure 4 shows that $\kappa \leqslant 2G$ in the validity regime of the dissipative plane for the phase transition. This bound on κ can be understood from equations (17) and (18). Since we have assumed $\Delta_q = \Delta_r = \Delta$ as the unit of frequency for our numerical work, equation (17) can be rewritten in the form $r_\pm = -2G \pm \sqrt{G^2(4+\Gamma^2) - (\kappa+\Gamma)^2}$. Clearly, $r_\pm$ will be complex if $\kappa > 2G\sqrt{(1+\Gamma^2/4)} - \Gamma$, implying that for $\Gamma = 0$ and $\kappa > 2G$, $r_\pm$ is complex. Now, upon substitution of equation (17) in (18), one can find that $\lambda_{c,-}$ also becomes complex when $r_\pm$ is complex.

3.3. Stability analysis

In general, the normal and superradiant solutions, equations (15) and (16), are not always stable. Therefore, it is necessary to investigate the stability of these solutions in both the normal and superradiant phases at the steady state. We carry out stability analysis using Lyapunov's indirect method. For a moderate strength of $\lambda_{c,-}$, we choose $\Gamma \simeq 0.1$ for stability analysis for different values of κ.

By considering the linear perturbation of the steady-state value $\langle \vec{\mathcal{V}} \rangle$, we expand the operator $\vec{\mathcal{V}}$ from the linearizing equation (14) as follows

$$\vec{\mathcal{V}} \equiv \{Q, P, X, Y, Z\}^T = \langle \vec{\mathcal{V}} \rangle + \delta\vec{\mathcal{V}} \tag{19}$$

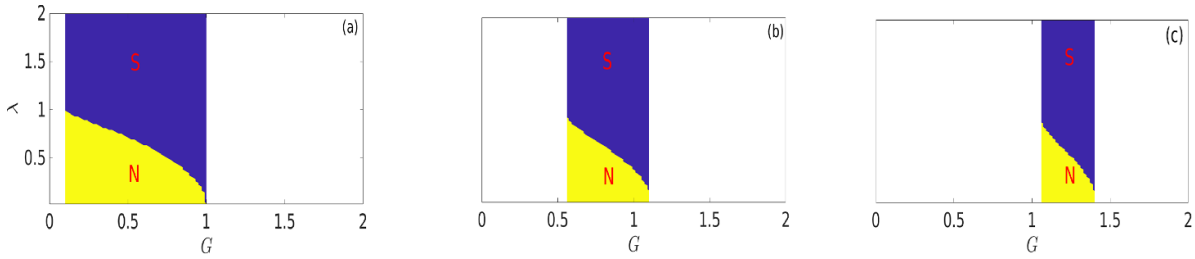


Figure 5. The stability of the normal and superradiant phases as a function of the drive strength G and coupling strength λ with (a) $\kappa = 0.1$, (b) $\kappa = 1$ and (c) $\kappa = 2$, keeping Γ fixed at 0.1. Stable regimes of the normal phase (N) and superradiant phase (SP) are clearly marked with yellow and blue colours, respectively. The white part depicts the nonphysical nature of the steady-state solutions, equations (15) and (16). Here, we do not distinguish between the mono-stable or bi-stable phases.

where $\delta\mathcal{V} = \sqrt{\langle\vec{\mathcal{V}}^2\rangle - \langle\vec{\mathcal{V}}\rangle^2}$ as the quantum fluctuation of $\vec{\mathcal{V}}$. For the normal phase, we have

$$\partial_t\vec{\mathcal{V}} = \partial_t(\delta\vec{\mathcal{V}}) = M_{NP}\delta\vec{\mathcal{V}}$$
$$= \begin{pmatrix} -\frac{\kappa}{2} & (\Delta_r - G) & 0 & -\sqrt{2}\lambda & 0 \\ -(\Delta_r + G) & -\frac{\kappa}{2} & -\sqrt{2}\lambda & 0 & 0 \\ 0 & \frac{\lambda}{\sqrt{2}} & -\frac{\Gamma}{2} & -\Delta_q & 0 \\ \frac{\lambda}{\sqrt{2}} & 0 & \Delta_q & -\frac{\Gamma}{2} & 0 \\ 0 & 0 & 0 & 0 & -\Gamma \end{pmatrix} \delta\vec{\mathcal{V}} \tag{20}$$

and for the superradiant phase

$$\partial_t\vec{\mathcal{V}} = \partial_t(\delta\vec{\mathcal{V}}) = M_{SP}\delta\vec{\mathcal{V}}$$
$$= \begin{pmatrix} -\frac{\kappa}{2} & (\Delta_r - G) & 0 & -\sqrt{2}\lambda & 0 \\ -(\Delta_r + G) & -\frac{\kappa}{2} & -\sqrt{2}\lambda & 0 & 0 \\ 0 & -\sqrt{2}\lambda Z_{SP} & -\frac{\Gamma}{2} & -\Delta_q & -\sqrt{2}\lambda P_{SP} \\ \sqrt{2}\lambda Z_{SP} & 0 & \Delta_q & -\frac{\Gamma}{2} & \sqrt{2}\lambda Q_{SP} \\ \sqrt{2}\lambda Y_{SP} & \sqrt{2}\lambda X_{SP} & \sqrt{2}\lambda P_{SP} & \sqrt{2}\lambda Q_{SP} & -\Gamma \end{pmatrix} \delta\vec{\mathcal{V}}. \tag{21}$$

Only if all the eigenvalues of $M_{NP(SP)}$ have negative real parts, then this normal (superradiant) phase is stable; otherwise, this solution is unstable.

In figure 5, we plot these eigenvalues in the $\lambda - G$ plane that shows $Z_{SP,-}$ for stable phases only for three different values of κ. The normal phase is illustrated by the yellow region in figure 5, whereas the blue area represents the superradiant phase. For $\kappa = 0.1$, we find that the semi-classical mean-field equation (14) provides a stable regime for (SP, NP). For $\kappa = 1$, the stable zone of (SP, NP) is shifted to the right, and its width is also reduced. The stable zone of (SP, NP) becomes narrow in the presence of large $\kappa = 2$ with similar characteristics to the previous one. Therefore, the larger cavity decay rate κ causes vanishing of the stable zone of (SP, NP). Indeed, the higher value of the cavity photon loss must be compensated by the larger drive strength in such a way that the system itself survives and does not move far from its stable zone. This feature allows the normal–superradiant transition in the presence of a wide range of values for the drive and dissipation. However, apart from the phase transition depicted by the yellow–blue colour in figure 5, the entire white region describes the nonphysical regime due to either $\mathrm{Im}(Z_{SP,-}) \neq 0$ or $Z_{SP,-} > 0$.

Undoubtedly, the unstable character of the mean-field steady-state solutions is entirely absent during normal to SPT, as can be seen from figure 5. Since we have focused only on the stable–unstable zone of (NP, SP), we do not discuss further mono-stable or bi-stable solutions. It is to be noted that the superradiant phase is always physically unstable, corresponding to $Z_{SP,+}$ and λ_c (defined in equation (18)), associated with a discontinuity in the unstable regime.

The solutions, equations (15) and (16), associated with the variable $Z_{SP,-}$ will always be stable for a broad range of system parameters. It is to be pointed out that $Z_{SP,-}$ also shows a discontinuity in a region, but the system exhibits the phase transition before arriving at the discontinuity for $Z_{SP,-}$. Therefore, the existence of discontinuity poses no difficulty, and we can explore the phase transition with the solution provided by $Z_{SP,-}$. The fact is that a discontinuity must appear in an unstable regime with the solutions governed by $Z_{SP,+}$. For this reason, we determine the stable solutions provided by only $Z_{SP,-}$.

Having established the existence of a normal–SPT, we display the cavity field amplitude $|\psi|$ in the $\lambda - G$ plane in figure 6 that conforms with the stability analysis of figure 5. In figure 6, the normal phase and superradiant phase are both separated by a boundary (the curved dashed magenta line) within the coloured area. The entire white region and the horizontal dashed magenta line describe the nonphysical behaviour of the steady-state solutions, equations (15) and (16), which is reflected in the stability analysis diagram in figure 5. It is obvious that the normal phase is given by $\psi = 0$, whereas $\psi \neq 0$ reveals the superradiant phase. With the increasing cavity decay rate κ, the phase transition regime itself is gradually shifted towards the higher drive strength G.

In figure 7, we plot the steady-state average values of $Z_{\pm}$ as a function of G. We explain figure 7 using figure 5. The results show the existence of the normal to superradiant transition with violation of the $\mathbb{Z}_2$ symmetry. Remarkably, the cavity decay rate κ breaks the $\mathbb{Z}_2$ symmetry more effectively and enhances the separation of the $Z_{\pm}$ curves. As shown in figures 7(a)–(c), due to $\lambda < \lambda_{c,-}$, the system is initially in a normal state up to a certain value of G. As previously illustrated in figure 6, as G increases, the critical coupling strength λ_c decreases gradually. As a result, the system is no longer in a normal state and has moved to a superradiant state. The system exhibits the normal to superradiant transition described by

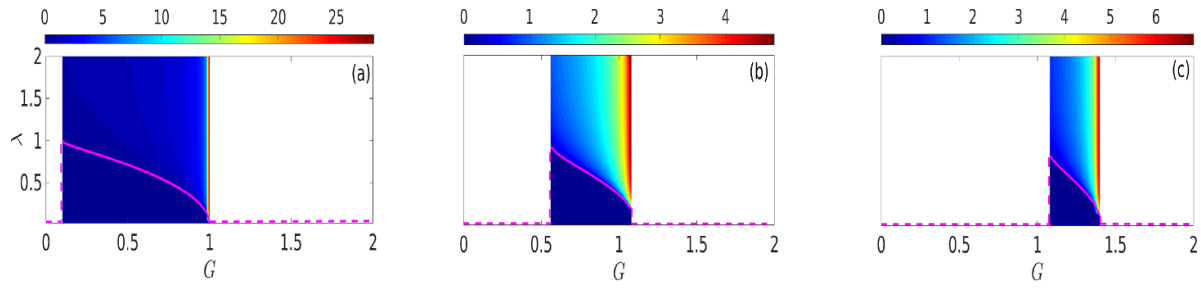


Figure 6. The ψ as a function of G and λ for (a) $\kappa = 0.1$, (b) $\kappa = 1$, and (c) $\kappa = 2$ and $\Gamma = 0.1$. Stable regimes of the normal and superradiant phase are marked by yellow and blue areas, respectively. The white parts with the horizontal dashed magenta lines depict the nonphysical steady-state solutions of the system. The dashed magenta lines indicate the boundary from the normal phase to the superradiant phase.

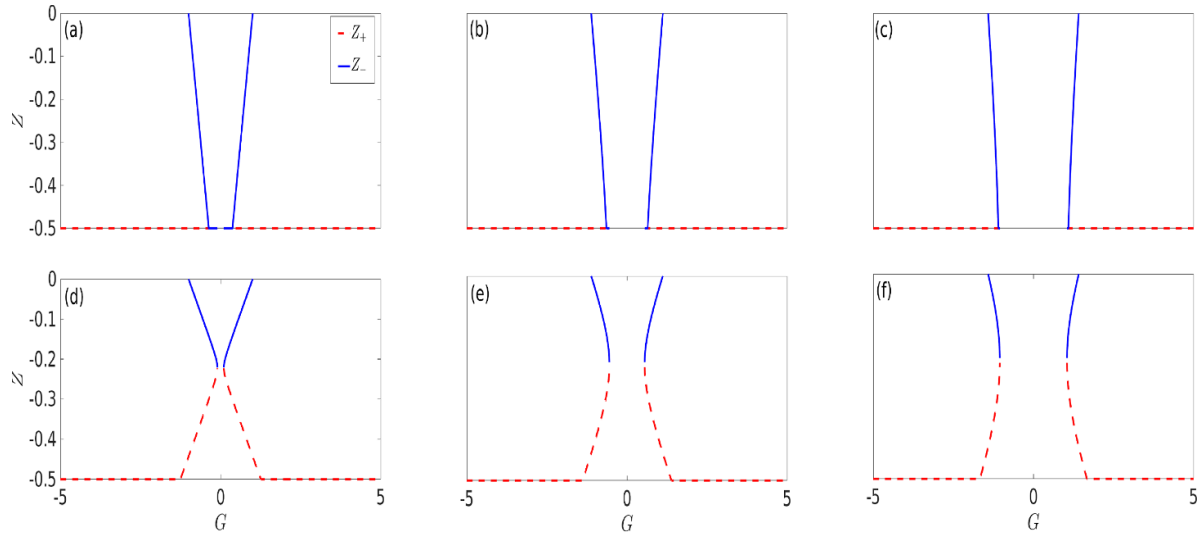


Figure 7. The steady-state order parameters $Z_\pm$ are plotted as a function of G for $\Gamma = 0.1$ with $\lambda = 0.8$ (top row) and $\lambda = 1.5$ (bottom row); (a), (d) $\kappa = 0.1$; (b), (e) $\kappa = 1$; (c), (f) $\kappa = 2$. The blue solid line is Z_- and the red dashed line indicates Z_+. For the top row, the blue solid line implies the normal–superradiant transition and the red dashed line represents only the superradiant state.

Z_-, whereas another solution Z_+ results in only the superradiant phase. In figures 7(d)–(f), we choose $\lambda = 1.5$, and observe that Z_+ itself is responsible for SPT in sharp contrast to the former case with $\lambda = 0.8$.

3.4. Collective modes

To diagonalize an interacting spin or spin-boson coupled system, one can employ either Jordan–Wigner (JW) or HP [46] transformation. HP transformation is usually used to diagonalize atom–photon or spin–boson interacting systems without any atom–atom or spin–spin interaction, while JW transformation is most useful in interacting spins or two-level atoms [55]. HP transformation renders a spin–boson coupled model into a complete bosonic model. In the case of non-interacting atoms, as in the present context, JW transformation will replace the total fermion number operator by the collective spin J_z. The resulting photon–atom model will then involve both fermion and boson statistics. It is difficult to deal with such a fermion–boson model with an open quantum-system formalism in contrast to a completely bosonic model after HP transformation. Furthermore, the fermion–boson model will not be parity conserved due to explicit dependence on the excitation number [55]. We therefore resort to HP transformation to map the collective spin operator into a bosonic one. The TC model can then be approximated as two coupled harmonic oscillators [48, 49]. One can rewrite the collective atomic operators $\hat{J}_+$, $\hat{J}_-$, and $\hat{J}_z$ in terms of the annihilation and creation operators, $\hat{b}$ and $\hat{b}^\dagger$, of a single bosonic mode

$$\hat{J}_z = \hat{b}^\dagger \hat{b} - \frac{N_q}{2} \tag{22}$$

$$\hat{J}_- = \sqrt{N_q - \hat{b}^\dagger \hat{b}}\, \hat{b} \tag{23}$$

$$\hat{J}_+ = \hat{b}^\dagger \sqrt{N_q - \hat{b}^\dagger \hat{b}}. \tag{24}$$

These bosonic operators describe magnon-like collective modes [56] of the system. Using $[\hat{b}, \hat{b}^\dagger] = 1$ and these transformations in equation (5), we obtain the effective Hamiltonian,

$$\hat{\mathcal{H}}_{eff} = \Delta_r \hat{a}^\dagger \hat{a} + \Delta_q (\hat{b}^\dagger \hat{b} - N_q/2) + \lambda \left(\hat{a} \hat{b}^\dagger \sqrt{1 - \hat{b}^\dagger \hat{b}/N_q} + \hat{a}^\dagger \sqrt{1 - \hat{b}^\dagger \hat{b}/N_q}\, \hat{b} \right) + \frac{G}{2} \left(\hat{a}^{\dagger 2} + \hat{a}^2 \right). \tag{25}$$

After expansion in the large N_q limit ($\langle \hat{b}^\dagger \hat{b} \rangle << N_q$), the Hamiltonian, equation (25), reduces to that of two coupled harmonic oscillators, as given by

$$\hat{\mathbb{H}} = \Delta_r \hat{a}^\dagger \hat{a} + \Delta_q \hat{b}^\dagger \hat{b} + \lambda(\hat{a}\hat{b}^\dagger + \hat{a}^\dagger \hat{b}) + \frac{G}{2}\left(\hat{a}^{\dagger 2} + \hat{a}^2\right). \quad (26)$$

Within the master equation approach, one has

$$\frac{d\hat{\rho}}{dt} = -i\left[\hat{\mathbb{H}}, \hat{\rho}\right] + \frac{\kappa}{2}\mathcal{D}[\hat{a}]\hat{\rho} + \frac{\Gamma}{2}\mathcal{D}[\hat{b}]\hat{\rho}. \quad (27)$$

In the preceding section, we analyzed the normal–superradiant transition to resolve the steady-state average values of various moments. However, this type of phase transition can also be investigated for the two coupled harmonic oscillators [48, 49] driven by a two-photon drive. Equation (27) provides two linear equations of motion for the average values of the operators $\hat{a}$ and $\hat{b}$,

$$\begin{cases} \frac{d}{dt}\langle \hat{a} \rangle = -\left(i\Delta_r + \frac{\kappa}{2}\right)\langle \hat{a} \rangle - i(\lambda \langle \hat{b} \rangle + G\langle \hat{a}^\dagger \rangle) \\ \frac{d}{dt}\langle \hat{b} \rangle = -\left(i\Delta_q + \frac{\Gamma}{2}\right)\langle \hat{b} \rangle - i\lambda \langle \hat{a} \rangle. \end{cases} \quad (28)$$

We solve the equations

$$\dot{\mathbf{V}} = A\mathbf{V}, \quad (29)$$

with $\mathbf{V} = (\langle \hat{a} \rangle, \langle \hat{a}^\dagger \rangle, \langle \hat{b} \rangle, \langle \hat{b}^\dagger \rangle)^T$ and

$$A = \begin{pmatrix} -\left(i\Delta_r + \frac{\kappa}{2}\right) & -iG & -i\lambda & 0 \\ iG & \left(i\Delta_r - \frac{\kappa}{2}\right) & 0 & i\lambda \\ -i\lambda & 0 & -\left(i\Delta_q + \frac{\Gamma}{2}\right) & 0 \\ 0 & i\lambda & 0 & \left(i\Delta_q - \frac{\Gamma}{2}\right) \end{pmatrix}. \quad (30)$$

Starting from the Heisenberg equations of motion for our set of operators $\mathbf{V}$, it is necessary to obtain the retarded Green's functions corresponding to $\mathbf{V}$. Our goal is to find the retarded Green's function defined by

$$\mathcal{G}^R_{l,m}(t) = -i\left\langle \left[V_l(t), V^\dagger_m(0)\right]\right\rangle \phi(t). \quad (31)$$

We define a constant matrix in terms of the equal-time correlation function, which is $\eta_{l,m} = \langle \left[V_l(0), V^\dagger_m(0)\right]\rangle$. In our case, only the diagonal elements survive for the two-mode operators ($\hat{a}$, $\hat{b}$) in the constant B-matrix, which is

$$\eta = \begin{pmatrix} 1 & 0 & 0 & 0 \\ 0 & -1 & 0 & 0 \\ 0 & 0 & 1 & 0 \\ 0 & 0 & 0 & -1 \end{pmatrix}. \quad (32)$$

The dynamical evolution of the retarded Green's function is given by

$$\frac{d}{dt}\mathcal{G}^R_{l,m}(t) = -i\delta(t)\eta_{l,m} + A_{l,p}\mathcal{G}^R_{p,m}(t). \quad (33)$$

As an example of Fourier transformation for an arbitrary function $h(\bullet)$, we can write

$$h(\omega) = \int_{-\infty}^{\infty} dt e^{i\omega t} h(t), \quad (34)$$

and we apply this transformation to equation (33) and obtain

$$\begin{aligned} (A + i\omega)\mathcal{G}^R(\omega) &= i\eta \\ [\mathcal{G}^R(\omega)]^{-1} &= \eta(\omega - iA). \end{aligned} \quad (35)$$

Substituting equations (30) and (32) into equation (35), we get

$$[\mathcal{G}^R(\omega)]^{-1} = \begin{pmatrix} \omega - \Delta_r + i\frac{\kappa}{2} & -G & -\lambda & 0 \\ -G & -\omega - \Delta_r - i\frac{\kappa}{2} & 0 & -\lambda \\ -\lambda & 0 & \omega - \Delta_q + i\frac{\Gamma}{2} & 0 \\ 0 & -\lambda & 0 & -\omega - \Delta_q - i\frac{\Gamma}{2} \end{pmatrix}. \quad (36)$$

At a certain value of interaction strength, e.g. $\lambda = \lambda_c$, the system exhibits the superradiant transition under the conditions $|[\mathcal{G}^R(\omega = 0)]^{-1}| = 0$. Therefore, the critical value is

$$\lambda_{c,\pm} = \pm\sqrt{\left(\Delta_q\Delta_r - \frac{\kappa\Gamma}{4}\right) \pm \sqrt{\left(\Delta_q\Delta_r - \frac{\kappa\Gamma}{4}\right)^2 - \left(\Delta_r^2 + \frac{\kappa^2}{4} - G^2\right)\left(\Delta_q^2 + \frac{\Gamma^2}{4}\right)}}. \quad (37)$$

In the limit G, κ, $\Gamma \to 0$, equation (37) recovers the zero-temperature limit of the equilibrium coupling strength result, $\lambda_c = \sqrt{\Delta_q \Delta_r}$. Undoubtedly, the critical value, equation (37), of the normal–superradiant transition through HP approximation is exactly the same, equation (18), as that obtained from the semi-classical steady-state analysis of the Heisenberg equations of motion (14).

4. Conclusions

In conclusion, we have presented a detailed study on the dissipative or non-equilibrium normal–SPT, the stability of the phases, and the associated collective phenomena of an open TC model driven by a two-photon drive. We have analyzed our results using dissipative phase diagrams depicting the effects of the decay of both the cavity mode and the qubits on the phases. Our results show that the critical coupling strength for the phase transition can be significantly reduced in the driven dissipative TC model compared to that for the non-dissipative model. We have shown that the breaking of the $\mathbb{Z}_2$ symmetry is more prominent due to the combined effects of the drive and the cavity decay. Recent experiments [13, 32] with a single-photon drive have demonstrated SPT in a regime where the drive strength and κ are smaller than Δ. However, in a dissipative TC model with a two-photon drive, as studied here, one may achieve SPT even for large values of G and κ, as our results reveal. Therefore, for the sake of completeness, we have presented the results for small to large values of these two parameters. In the thermodynamic limit of $N_q \to \infty$, the use of HP transition transforms the Hamiltonian into that of two coupled oscillators driven by a two-photon drive, where one oscillator corresponds to the cavity mode and the other to the spin wave. Such a model is known to give rise to two-mode squeezing [57] and entanglement [58, 59]. It would be interesting to explore the effects of dissipation and two-photon drive on the cavity–spin–wave entanglement across the dissipative phase transition.

The open TC model described in this paper may serve as a fundamental premise for investigating the polariton spectrum [55]. Besides this, our model may be tweaked to mimic light–matter interaction for an open quantum battery [60–62].

Data availability statement

All data that support the findings of this study are included within the article (and any supplementary files).

ORCID iDs

Kingshuk Adhikary https://orcid.org/0000-0003-0034-9889
Özgür E Müstecaplıoğlu https://orcid.org/0000-0002-9134-3951
Bimalendu Deb https://orcid.org/0000-0002-7036-8391

References

[1] Hepp K and Lieb E H 1973 *Ann. Phys., NY* **76** 360–404
[2] Wang Y K and Hioe F T 1973 *Phys. Rev.* A **7** 831–6
[3] Hioe F T 1973 *Phys. Rev.* A **8** 1440–5
[4] Hepp K and Lieb E H 1973 *Phys. Rev.* A **8** 2517–25
[5] Dicke R H 1954 *Phys. Rev.* **93** 99–110
[6] Garraway B M 2011 *Phil. Trans. R. Soc.* A **369** 1137–55
[7] Kirton P, Roses M M, Keeling J and Dalla Torre E G 2019 *Adv. Quantum Technol.* **2** 1800043
[8] Torre E G D, Diehl S, Lukin M D, Sachdev S and Strack P 2013 *Phys. Rev.* A **87** 023831
[9] Brennecke F, Mottl R, Baumann K, Landig R, Donner T and Esslinger T 2013 *PNAS* **110** 11763–7
[10] Nagy D, Kńya G, Szirmai G and Domokos P 2010 *Phys. Rev. Lett.* **104** 130401
[11] Link V and Strunz W T 2020 *Phys. Rev. Lett.* **125** 143602
[12] Klinder J, Keßler H, Wolke M, Mathey L and Hemmerich A 2015 *PNAS* **112** 3290–5
[13] Baumann K, Guerlin C, Brennecke F and Esslinger T 2010 *Nature* **464** 1301–6
[14] Tavis M and Cummings F W 1968 *Phys. Rev.* **170** 379–84
[15] Tavis M and Cummings F W 1969 *Phys. Rev.* **188** 692–5
[16] Walls D F and Milburn G J 1995 *Quantum Optics* Springer Study Edition (Berlin: Springer)
[17] Chen Q-H, Zhang Y-Y, Liu T and Wang K-L 2008 *Phys. Rev.* A **78** 051801
[18] Larson J and Irish E K 2017 *J. Phys. A: Math. Theor.* **50** 174002
[19] Baksic A and Ciuti C 2014 *Phys. Rev. Lett.* **112** 173601
[20] Dimer F, Estienne B, Parkins A S and Carmichael H J 2007 *Phys. Rev.* A **75** 013804
[21] Viehmann O, von Delft J and Marquardt F 2011 *Phys. Rev. Lett.* **107** 113602
[22] Fink J M, Bianchetti R, Baur M, Göppl M, Steffen L, Filipp S, Leek P J, Blais A and Wallraff A 2009 *Phys. Rev. Lett.* **103** 083601
[23] Hwang M-J, Puebla R and Plenio M B 2015 *Phys. Rev. Lett.* **115** 180404
[24] Ashhab S 2013 *Phys. Rev.* A **87** 013826
[25] Hwang M-J and Plenio M B 2016 *Phys. Rev. Lett.* **117** 123602
[26] Zhang Y-Y, Hu Z-X, Fu L, Luo H-G, Pu H and Zhang X-F 2021 *Phys. Rev. Lett.* **127** 063602
[27] Padilla D F, Pu H, Cheng G-J and Zhang Y-Y 2022 *Phys. Rev. Lett.* **129** 183602
[28] Genes C, Berman P R and Rojo A G 2003 *Phys. Rev.* A **68** 043809
[29] Ma J-M, Jiao Z-Y and Li N 2008 *Int. J. Theor. Phys.* **47** 1270–7
[30] Abdalla M S, Hassan S S and Obada A -S F 1986 *Phys. Rev.* A **34** 4869–74
[31] Zou J H, Liu T, Feng M, Yang W L, Chen C Y and Twamley J 2013 *New J. Phys.* **15** 123032
[32] Feng M, Zhong Y, Liu T, Yan L, Yang W L, Twamley J and Wang H 2015 *Nat. Commun.* **6** 7111
[33] Zhang Y Q and Xu J B 2011 *Eur. Phys. J.* D **64** 549–55
[34] Ollivier H and Zurek W H 2001 *Phys. Rev. Lett.* **88** 017901
[35] Soriente M, Donner T, Chitra R and Zilberberg O 2018 *Phys. Rev. Lett.* **120** 183603
[36] Zhu C J, Ping L L, Yang Y P and Agarwal G S 2020 *Phys. Rev. Lett.* **124** 073602
[37] Tessier T E, Deutsch I H, Delgado A and Fuentes-Guridi I 2003 *Phys. Rev.* A **68** 062316
[38] Wang Y, Wu J-L, Song J, Zhang Z-J, Jiang Y-Y and Xia Y 2020 *Phys. Rev.* A **101** 053826
[39] Youssef M, Metwally N and Obada A-S F 2010 *J. Phys. B: At. Mol. Opt. Phys.* **43** 095501

[40] Ma J-M, Jiao Z-Y and Li N 2007 *Int. J. Theor. Phys.* **46** 2550–9
[41] Retzker A, Solano E and Reznik B 2007 *Phys. Rev.* A **75** 022312
[42] Alodjants A P, Bazhenov A Y, Khrennikov A Y and Bukhanovsky A V 2022 *Sci. Rep.* **12** 8566
[43] Bazhenov A Y, Nikitina M and Alodjants A P 2022 *Opt. Lett.* **47** 3119–22
[44] Guerra C A E, Mahecha-Gḿez J and Hirsch J G 2020 *EPJD* **74** 140502
[45] Emary C and Brandes T 2003 *Phys. Rev.* E **67** 066203
[46] Holstein T and Primakoff H 1940 *Phys. Rev.* **58** 1098–113
[47] Ressayre E and Tallet A 1975 *Phys. Rev.* A **11** 981–8
[48] Estes L E, Keil T H and Narducci L M 1968 *Phys. Rev.* **175** 286–99
[49] Makarov D N 2018 *Phys. Rev.* E **97** 042203
[50] Kosloff R and Levy A 2014 *Annu. Rev. Phys. Chem.* **65** 365–93
[51] Sun K W, Li R and Zhang G F 2017 *EPJD* **71** 174002
[52] Hardal A C and Müstecaplıoğlu E 2015 *Sci. Rep.* **5** 12953
[53] Johansson J, Nation P and Nori F 2012 *Comput. Phys. Commun.* **183** 1760–72
[54] Sheshadri K, Krishnamurthy H R, Pandit R and Ramakrishnan T V 1993 *Europhys. Lett.* **22** 257–63
[55] Cortese E, Garziano L and De Liberato S 2017 *Phys. Rev.* A **96** 053861
[56] Galkin A Y, Ivanov B A and Zaspel C E 2006 *Phys. Rev.* B **74** 144419
[57] Sebawe Abdalla M 1991 *Physica* A **179** 131–44
[58] Huang H and Agarwal G S 1994 *Phys. Rev.* A **49** 52–60
[59] Agarwal G S and Banerji J 2006 *J. Phys. A: Math. Gen.* **39** 11503
[60] Barra F 2019 *Phys. Rev. Lett.* **122** 210601
[61] Gherardini S, Campaioli F, Caruso F and Binder F C 2020 *Phys. Rev. Res.* **2** 013095
[62] Quach J Q and Munro W J 2020 *Phys. Rev. Appl.* **14** 024092